

The Physical Origin of Extreme Emission Line Galaxies at High Redshifts: Strong [OIII] Emission Lines Produced by Obscured AGNs

CHENGHAO ZHU^{1,2} YUICHI HARIKANE³,¹ MASAMI OUCHI^{3,1,4,5} YOSHIAKI ONO⁶,¹ MASATO ONODERA^{7,4,6}
 SHENLI TANG^{8,7} YUKI ISOBE^{9,8} YOSHIKI MATSUOKA⁹ TOSHIHIRO KAWAGUCHI¹⁰ HIROYA UMEDA,^{1,2}
 KIMIHIKO NAKAJIMA^{11,3} YONGMING LIANG¹¹ YI XU^{11,11} YECHI ZHANG^{11,3} DONGSHENG SUN^{11,11}
 KAZUHIRO SHIMASAKU¹² JENNY GREENE,¹³ KAZUSHI IWASAWA^{14,15} KOTARO KOHNO,¹⁶ TOHRU NAGAO,^{17,18}
 ANDREAS SCHULZE,³ TAKATOSHI SHIBUYA,¹⁹ MIFTAHUL HILMI^{20,21} AND MALTE SCHRAMM³

1. Introduction

- Extreme Emission Line Galaxies (EELGs) are characterized by very strong [OIII] emission lines (equivalent width $EW > 2000 \text{ \AA}$)
 - which are generally considered to be indicators of strong star formation activity.
- In some high redshift EELGs, very strong [OIII] emission lines may be induced by obscured active galactic nuclei (AGN) rather than star formation.

2. Observation

- Observed two EELGs at redshift $z = 0.828, 0.728$ with the Subaru/FOCAS spectrum (ID: J1000+0211, J0845-0123)
 - equivalent widths of the [OIII] $\lambda 5007$ emission line were measured to be about 2905 \AA and 2000 \AA , respectively
- Additionally, an EELG at $z \approx 2.055$ was analyzed by the JWST CEERS program (ID: CEERS-3506)
 - equivalent width of the [OIII] emission line is about 2508 \AA
- All three galaxies showed very strong emission lines with equivalent widths (EWs) of the [OIII] $\lambda 5007$ emission line reaching 2000–2900 \AA
- It is difficult to explain with existing star formation models.

3. Result

- By analyzing the spectral and luminosity properties of three extreme emission line galaxies (EELGs), they suggest that their strong [OIII] $\lambda 5007$ emission line may be driven by an obscured active galactic nucleus (AGN).

3.1 Emission Lines

3.1.1 Balmer Decrement

- Dust attenuation was assessed using the ratios of the Balmer lines ($H\gamma/H\beta, H\delta/H\beta$)
- measured ratios in all three galaxies were in agreement with the theoretical ratios, indicating that dust attenuation is minimal.

3.1.2 Chemical Properties

- All three galaxies show low metallicity ($12 + \log(O/H) \approx 7.5-8.0$)
- consistent with a strong [OIII] emission line.

3.1.3 Line Diagnostics

- Using the BPT diagram and the blue diagram to evaluate whether there are AGNs (Figure 3)
- All three galaxies are located on the border between star-forming regions and AGN regions
 - it is difficult to clearly determine the presence of AGNs using optical line diagnostics.

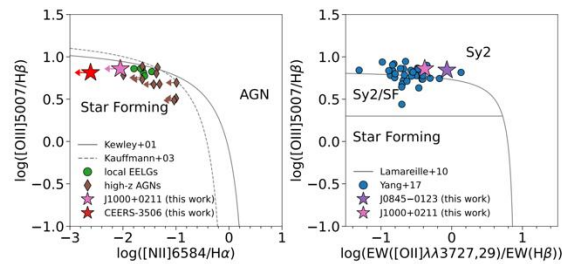


Figure 3. BPT diagram (left) and the blue diagram (right) for our objects. **The left panel:** the red and pink stars denote the results of J1000+0211 and CEERS-3506 measured in this work, respectively. The green circles represent local EELGs (Jaskot & Ouy 2013). The brown diamonds represent high-z AGNs from Harikane et al. (2023) and Chisholm et al. (2024). We use the arrows if only upper limits can be constrained. The solid and dashed lines are the separation lines recommended by Kewley et al. (2001) and Kauffmann et al. (2003), respectively. **The right panel:** the purple and pink stars denote the results of J0845-0123 and J1000+0211 measured in this work, respectively. The blue circles denote the “blueberry” galaxies with high EW([OIII]) from Yang et al. (2017). The solid lines are the separation lines suggested in Lamareille (2010). Similar to local EELGs and high-z AGNs, our objects are located on the border between the star formation and AGN regions in both diagrams.

3.2 Broad Component Identification

3.2.1 [OIII] $\lambda 5007$ lines

- Analysis of the [OIII] $\lambda 5007$ line profile to assess the presence of broad components
 - revealed that broad components were detected in J0845-0123 and CEERS-3506

3.2.2 H β lines

- Analysis of the H β line did not detect a broad component in any of the three galaxies,
 - which could indicate that the broad line region (BLR) of the AGN is obscured or that the AGN is weak.

3.2.3 Other lines of CEERS-3506

- In CEERS-3506, broad components were also detected in the H α , He I $\lambda 10830$, and Pa β lines, further supporting the presence of AGN.

3.3 SED Fitting and Photometric Result (Figure 7)

- Analysis of the SEDs of J1000+0211 and CEERS-3506 reveals an excess in the near-infrared
 - suggesting the presence of an obscured AGN.
- In particular, in CEERS-3506, the infrared contribution of the AGN is as high as 60% of the total infrared luminosity
 - indicating a strong presence of the AGN.

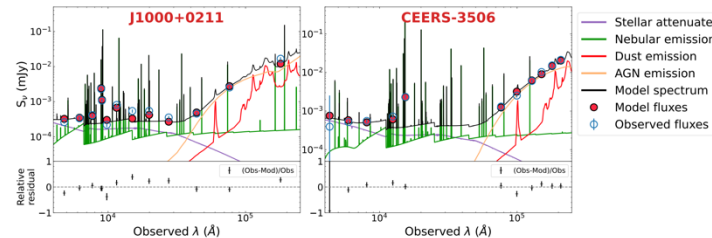


Figure 7. CIGALE SED fitting results of the two [OIII] emitters, J1000+0211 (left) and CEERS-3506 (right). The blue open and red filled circles mark the observed fluxes and the model fluxes, respectively. The solid lines mark the best-fit models of the total spectrum (black), stellar continuum (purple), nebular emission (green), AGN emission (orange; including emission from surrounding dust torus), and the dust emission (red; dust heated by stars). Both J1000+0211 and CEERS-3506 display the near-infrared excess ($\gtrsim 2 \mu\text{m}$ in the rest-frame) suggesting the existence of hidden AGN complemented by our spectroscopic measurements. The bottom panels are the relative residuals.

3.4 Surface Brightness Profiles (Figure 9)

- Analysis of the surface brightness profiles of J1000+0211 and CEERS-3506 shows that both galaxies have point-like profiles
 - suggesting the presence of an AGN at their centers.

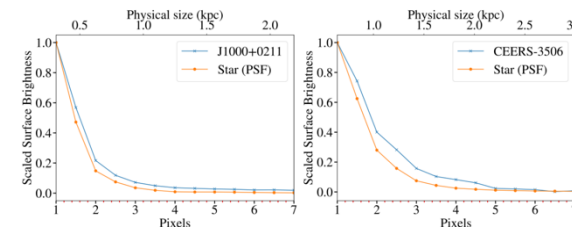


Figure 9. Surface brightness profiles (annuli) of CEERS-3506 (left) and J1000+0211 (right) compared with nearest stars. The blue crosses mark the surface brightness profiles within the evenly spaced annuli. The orange crosses denote the closest star representing PSF. The comparison is conducted with the ACS-F435W ($\lambda_0 : 0.13 - 0.16 \mu\text{m}$) image and NIRCam-F150W ($\lambda_0 : 0.73 - 0.91 \mu\text{m}$) image for CEERS-3506 and J1000+0211 respectively. The filters are chosen due to less contamination from the emission lines. This comparison reveals the compactness of J1000+0211 and CEERS-3506.

4. Discussion

4.1 AGN Properties

- Figure 11: Relationship between black hole mass and stellar mass of CEERS-3506 and J1000+0211
 - For CEERS-3506, the black hole mass was estimated using various methods (H α , Pa β emission line-based estimation, SED fitting)
 - For J1000+0211, it was estimated using SED fitting
- Their positions are similar to those of high-redshift AGNs, suggesting that they are AGN-dominated galaxies.

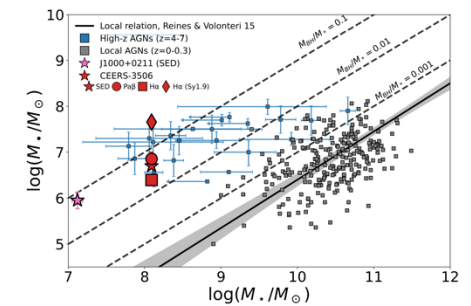


Figure 11. Relation between black hole mass (M_{bh}) and host's stellar mass (M_*). The red symbols mark the black hole mass of CEERS-3506 estimated by various methods (star: SED; by assuming $A_{\text{dust}} = 1$; circle: Pa β calibration; square: H α calibration; diamond: H α calibration with Sy1.9 correction). The pink star marks the estimation of J1000+0211 (SED, the same method as CEERS-3506). The blue squares are AGNs at $z = 4 - 7$ from Harikane et al. (2023) and Maslino et al. (2023). The gray squares mark the local AGNs from Chen et al. (2017) and Reines & Volonteri (2015). The black line is the local relation (Reines & Volonteri 2015) with 1 σ region marked by gray shade. The dashed lines denote the $M_*/M_{\text{bh}} = 0.001, 0.01$, and 0.1. This suggests that our studied objects are AGN-dominated and show more similarity to the AGNs at high redshift.

4.2 Physical Origins of High EW Objects

Using Cloudy modeling, they simulated spectra of stars and AGN with varying metal contents and ionization parameters.

- Figure 12: Relationship between EW [OIII] and stellar age in star formation models
 - Curves are included for various metal contents, and the positions of CEERS-3506, J1000+0211, and J08450123 are indicated.
 - This analysis shows that CEERS-3506 and J08450123 can be explained by the star formation model
 - J1000+0211 cannot be explained by the star formation model.
- Figure 13: Relationship between EW [OIII] and metallicity
 - This figure shows how the EW[OIII] varies with metallicity in the star formation model, the obscured AGN model, and the unobscured AGN model.
- Figure 12 shows that it cannot be explained by the star formation model. Therefore, it suggests that the obscured AGN model is more suitable for explaining high EW [OIII].

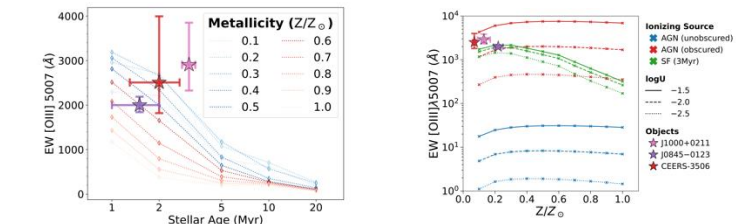


Figure 12. Relation between EW[OIII] and stellar population age for BPTB library model. Different colors represent various metallicity settings from 0.1 to 1 solar metallicity. The red, pink, and purple stars denote the CEERS-3506, J1000+0211, and J0845-0123, respectively. EW[OIII] decreases as the stellar age increases. The relation between EW[OIII] and metallicity is not monotonic. Our results agree well with Izzou (2011).

[Summary]

- Traditional optical line diagnostics, such as BPT diagrams, do not detect clear signs of active galactic nuclei (AGN).
- Analysis of the spectral energy distribution (SED) of three galaxies revealed near-infrared excess in two galaxies (J1000+0211, CEERS-3506), suggesting the presence of an obscured AGN
- The observed strong [OIII] emission line could not be reproduced from the spectrum of the star or the unobscured AGN. However, obscured AGN can explain it.
- Galaxy with a strong [OIII] emission line at high redshift epoch is likely an obscured AGN rather than a star forming galaxy.
- To accurately understand the physical origin of EELG, multiwavelength observations including infrared data as well as optical data are essential, and studies on more samples are needed in the future.